https://dx.doi.org/10.1016/j.jobe.2021.103151

Design optimization of multi-functional building envelope for thermal insulation and exhaust air heat recovery in different climates

Chong Zhang [a,b] *, Fu Xiao [b], Jinbo Wang [a] *

a. Department of Building Environment and Energy Engineering, Huazhong University of Science and Technology, Wuhan, China

b. Department of Building Services Engineering, The Hong Kong Polytechnic University, Hong Kong, China

Abstract

Exhaust air insulation wall (EAIW) utilizes the exfiltration process of low-grade exhaust air within porous material to improve the thermal insulation of wall. Previous studies tend to neglect the pressure loss of exfiltration process and its impact on optimal design of EAIW. This paper quantitatively estimates the pressure loss of exfiltration process and proposes a methodology to determine the optimal design for maximizing energy saving potential of EAIW. In this study, a network heat transfer model was validated and used to calculate the hourly cooling and heating load of EAIW. The pressure loss of exfiltration process and its related energy consumption was estimated by Darcy's law. The optimal design was identified for minimizing the overall annual energy consumption of EAIW in different climates. Influences of exfiltration velocity and porous material selection on the optimal design of EAIW were investigated. The results demonstrate the pressure loss of exfiltration process significantly affects the overall energy performance and optimal design of EAIW. The optimal thickness of porous material component are 40 mm, 50 mm, and 50 mm for three

climate zones, which correspond to a minimum annual overall energy consumption of 0.51 kWh/m^2, 0.48 kWh/m^2, and 0.49 kWh/m^2, respectively. The porous materials with high permeability and thermal resistance are recommended as air-permeable component of EAIW. The optimal design can achieve a trade-off between cooling/heating energy consumption and fan power consumption for maximizing the energy saving potential of EAIW.

Keywords: building envelope; thermal insulation; exhaust air heat recovery; porous materials; design optimization

Corresponding author: Chong Zhang
E-mail address: chong0324.zhang@polyu.edu.hk
Address: Department of Building Services Engineering, The Hong Kong Polytechnic University, Hong Kong, China

Corresponding author: Jinbo Wang
E-mail address: jbwang@hust.edu.cn
Address: Department of Building Environment and Energy Engineering, Huazhong University of Science and Technology, Wuhan 430074, China

Nomenclature

c	specific heat capacity, J/(kgK)
E	energy consumption, kWh/m^2
h	heat transfer coefficient, W/(m^{2}K)
H	height, m
k	permeability, m^2
L	thickness, m
N	number of the subsections
ΔP	pressure loss, Pa
Q	cumulative energy demand, kWh/m^2
T	temperature, K
W	width, m
v	exfiltration velocity, m/s
u	air velocity in air gap, m/s
ρ	density, kg/m^3
λ	thermal conductivity, W/mK
ε	emissivity
σ	Stefan-Boltzmann's constant, W/(m^{2}K^4)
μ	dynamic viscosity of air, Pa·s
τ	hourly time-step, h
EAIW	exhaust air insulation wall

HSCW hot summer and cold winter

HSWW hot summer and warm winter

MSE mean square error

MAPE mean absolute percentage error

Subscripts

a air

e exterior surface

i interior surface

in indoor/inside

j section j

m masonry structure

out outdoor/outside

p porous materials

r long-wave radiation

1 porous material component

2 air gap

3 masonry structure

1. Introduction

Nowadays, approximately 39 % and 36 % of the greenhouse gas (GHG) emissions and total energy use in the world are generated by building sector during its whole life-cycle [1]. Buildings are recognized as a significant sector for decreasing the global GHG emissions and total energy use. In recent years, great efforts have been devoted to research and develop the low-energy and sustainable building technologies, in terms of integrating the renewable energy sources into buildings [2], employing the emerging high-performance devices [3], developing novel building design method [4], applying data-driven modelling to improve building operation efficiency [5], guaranteeing indoor thermal environment through energy-efficient solution [6], enhancing the thermal insulation of building envelopes [7], and etc. Furthermore, building envelope accounts for 20% to 50% of cooling and heating loads of buildings [8]. This fact highlights the necessity of developing high-performance and energy-efficient building envelopes.

The heat gain/loss through building envelopes mainly result from the temperature difference between ambient and indoor environment. In general, a higher thermal resistance helps to reduce the unwanted heat transmission of the wall as well as the cooling and heating demand of buildings. Employing an insulation layer at external or internal surface of building envelope is the commonest approach to increase the thermal resistance [9]. Recently, super insulation materials such as advanced aerogel materials [10] and vacuum insulation panels (VIP) [11] with extremely low thermal conductivity have been developed to further minimize the heat gain/loss through building envelopes. Moreover, numerous investigations integrate

the phase change materials into building envelopes to moderate the fluctuation of its interior surface temperature and also decrease the peak load of building envelopes [12-14]. For the warm and tropical climates, some approaches are proposed to directly decrease the external surface temperature of building envelopes, and consequently the heat gain is significantly eliminated. Integrating vegetation systems into building envelopes, such as green wall [15] and green roof [16], can cool down the external surface of building envelopes in summer by the processes of thermal insulation, evaporative cooling, and solar shading. Furthermore, the transparent glazing systems are recognized as a pivotal role for achieving building energy saving and providing a satisfied indoor visual/thermal comfort. The heat transfer characteristics, key parameters, and energy performance of the glazing components have been exhaustively investigated [17-19].

Some innovative technologies are developed for integrating low-grade energy sources into building envelopes. Pipes-embedded building envelope utilizes the low-grade cooling or heating water obtained from ground heat exchanger [20], nocturnal radiative sky cooling [21], evaporative cooling [22], or air source heat pump [23], to circulate within the embedded pipes. The flowing low-grade water can release and remove heat inside the building envelopes in winter and summer, respectively, and then the heating and cooling loads are fully eliminated [24]. Radiative sky cooling provides an approach to loss heat to the outer space through thermal radiation without any energy consumption [25]. Nocturnal radiative sky cooling is commonly integrated with building envelopes. Such a design can significantly cool down the external surface of building envelope at night and achieve promising energy

saving potential in warm and tropical climates [26]. In recent years, the emerging scalable-manufactured glass-polymer hybrid metamaterial was proposed to show a significant potential of day and night radiative sky cooling [27]. Integrating this novel radiative sky cooling with the roof of single-family house in US can reduce 26.5%-76.1% annual cooling energy demands [28]. Moreover, building-integrated photovoltaics (BIPV) system can be regarded as a component of building envelopes for the entire building-skins [29], which can enhance building thermal insulation and also provide power generation. Furthermore, the ventilated wall allows the low-grade ambient air [30], outlet air of earth-to-air heat exchanger [31], or exhaust air from heating, ventilation, and air conditioning (HVAC) system [32] to flow through the channel inside the ventilated wall for avoiding overheating in summer and preventing heat loss in winter. Above these studies demonstrate that integrating the building envelopes with low-grade energy sources can effectively reduce the cooling and heating energy demands.

In general, the building external wall is air-impermeable. However, there is a kind of porous material based air-permeable building envelope, which allows the air to exfiltrate or infiltrate through the building envelope mechanically or passively for exhaust air heat recovery [33] or fresh air supply [34]. By effectively integrating building thermal insulation and ventilation, air-permeable building envelope becomes a promising method for achieving excellent thermal performance while improving indoor air quality.

1.1 Recent development and research gap on air-permeable building envelope

So far the air-permeable building envelope can be designed as infiltration mode or

exfiltration mode, as illustrated in Fig.1. For the infiltration mode, known as dynamic insulation or breathing wall [34], the fresh air permeates through the wall from outdoor to indoor in cold climates. The infiltration airflow can be preheated by recovering the conductive heat loss through the wall. For the exfiltration mode, called as exhaust air insulation wall (EAIW) [33], the low-grade exhaust air from HVAC system permeates through the wall from indoor to outdoor. Hence, the conductive heat flux from outdoor to indoor is removed and eliminated by the exfiltration airflow. For the practical application of the air-permeable building envelopes, a mechanical fan will be needed to provide a stable airflow.

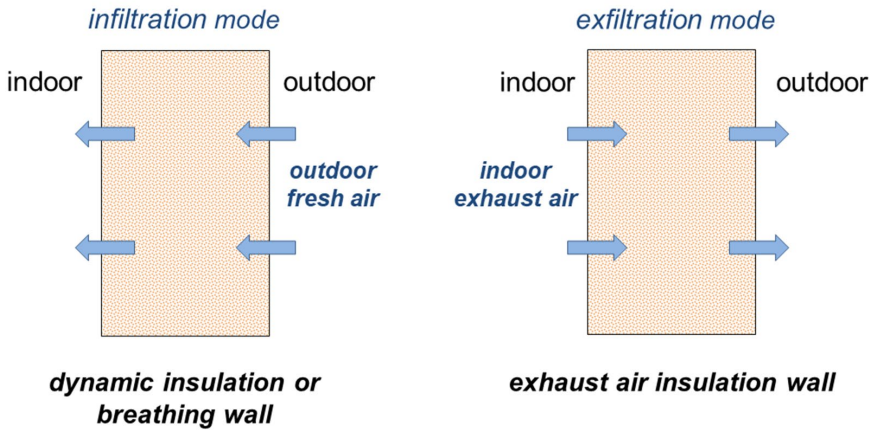

Fig. 1. Schematic of the air-permeable building envelope

Previous studies on air-permeable building envelope mainly focused on its thermal performance, impact on thermal comfort or indoor air quality (IAQ), filtration performance as well as application feasibility, and etc. Dalehaug et al. [35] reported that applying the dynamic insulation wall in a residential building can recover approximately half of conductive heat loss for preheating the ventilation air. Taylor and Imbabi [36] pointed out that the U-value of dynamic insulation could be decreased to near-zero by increasing infiltration

air rate and porous material thickness. Similar results can be observed in the study about the thermal performance of the EAIW carried out by Zhang et al. [37]. The results indicate that for a porous layer thickness of 30 mm and exfiltration airflow velocity of 0.003 m/s, the U-value of the EAIW would be reduced to less than 0.1 W/(m^2K). When the thickness reaches 50 mm, this value can be further reduced to almost 0 W/(m^2K). Dimoudi et al. [38] designed a test cell in Greece to investigate the operation mechanism and energy saving potential of a dynamic insulation wall under actual weather conditions. Gan [39] numerically explored the effects of air-filtration on the thermal environment in a room employed with dynamic insulation wall. Wong et al. [40] experimentally investigated the thermal conductivity of air-permeable dynamic concrete from a microscopic perspective. Moreover, researchers also focus on the filtration performance of dynamic insulation wall. Di Giuseppe et al. [41] carried out an experimental and analytical investigation on the filtration performance of a dynamic insulation wall for application in Italy climate. The results indicated that the unwanted particles in ventilation air will be filtered by porous material component during the infiltration process. Taylor et al. [42] pointed out that the dynamic insulation wall can act as a high-efficiency particulate air (HEPA) filter when the porous material thickness reaches to 60 mm. Ascione et al. [43] integrated the nocturnal free cooling with dynamic insulation for reducing indoor air temperature and improving thermal comfort in cooling season. In recent years, Alongi et al. [44-46] developed a specially designed laboratory apparatus to experimentally investigate the steady-state and unsteady-state thermal behavior of dynamic insulation module and further validate the classical analytical model and a novel steady

periodic analytical model. Craig and Grinham [47] conducted a schlieren imaging experiment to theoretically investigate the convective heat transfer mechanism at the surfaces of air-permeable porous material. Moreover, mass timber panels based dynamic insulation module was designed and optimized by Craig et al. [48] for reducing the embodied and operational carbon emissions of buildings.

It is observed that the porous material component acted as the core unit of air-permeable building envelopes can exchange heat with the infiltration or exfiltration airflow. Previous studies have proved the increase of porous material thickness can effectively reduce the U-value [36] and improve the heat recovery efficiency [37] as well as the filtration performance [42] of the air-permeable building envelopes. However, the infiltration or exfiltration process within the porous material component will lead to pressure loss to a certain degree and power consumption of a mechanical fan for supplying a constant airflow. This means that increasing the thickness of porous material will reduce the cooling and heating loads of the air-permeable building envelopes, and in the meanwhile, result in a higher pressure loss and additional fan power consumption. However, in previous studies the thickness of porous material was designed only according to the U-value or heat gain/loss of the wall. Few studies consider the impact of pressure loss and additional fan power consumption on the design of air-permeable building envelopes. Moreover, there are no guides and experiences on how to estimate the fan power consumption due to the infiltration or exfiltration process and its impact on the overall energy performance of the air-permeable building envelopes. Therefore, for the existing studies on the air-permeable building

envelopes, the designed and recommended thickness of the porous material may not be the optimal state from the viewpoint of achieving the minimum total energy consumption (air-conditioning and mechanical fan).

To accurately estimate the energy performance of the air-permeable building envelope, the pressure loss of exfiltration or infiltration process and its corresponding fan energy consumption should be considered. It is necessary to identify the optimal thickness of porous material component to minimize the overall energy consumption of the air-permeable building envelope.

1.2 Objectives of this study

To fully address the above critical challenges, the main objectives of this paper are to estimate the pressure loss of exfiltration process within porous material, propose a methodology to identify the optimal thickness of porous material for minimizing the overall energy consumption, and provide a recommended design guideline of the air-permeable building envelope. In this study, a comprehensive methodology was proposed to evaluate the overall energy performance of the EAIW, which is composed of three components, including the energy demands of cooling, heating, and additional mechanical fan due to the pressure loss of exfiltration process. A network heat transfer model of the EAIW was proposed and used to estimate its hourly cooling or heating energy demand. The model was verified by comparing the measurement data and corresponding computational results. A Darcy's law-based pressure model was used to estimate the pressure loss of the exfiltration process within porous material, and to further estimate the fan power consumption for driving a

constant exfiltration airflow of the EAIW. The optimal thickness of porous material component was determined according to the minimum annual overall energy consumption of the EAIW in different climate zones including hot summer and warm winter (HSWW) climate, hot summer and cold winter (HSCW) climate, and cold climate. Moreover, influence of some key parameters such as the exfiltration velocity and permeability of porous materials on the optimal design and overall annual energy performance of the EAIW was investigated quantitatively. The outcomes of this study will provide a more comprehensive evaluation method and optimal design guideline for this multi-functional air-permeable building envelope.

2. Methodology

This section presents and elaborates a simulation method to analyze the overall energy performance and optimal design of the EAIW. The research methodology for optimal design mainly includes the following parts: (1) developing and validating the heat transfer model to evaluate the hourly and annual cooling and heating energy demands of EAIW; (2) estimating the pressure loss based on Darcy's law and the corresponding fan power consumption of EAIW; (3) carrying out the sensitivity analysis to identify the optimal parameter for achieving the minimum overall energy consumption. The research methodology is illustrated in Fig. 2 and detailly introduced step by step as follows.

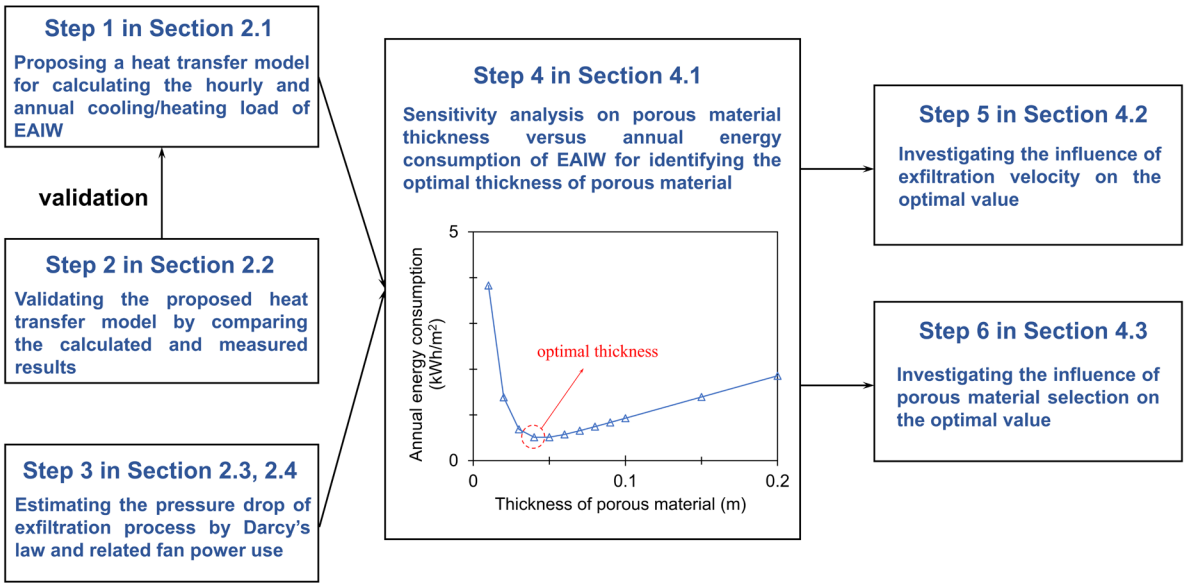

Fig. 2. Research methodology for design optimization of EAIW

2.1 Physical and mathematical heat transfer model

Fig. 3 presents the schematic and insulation mechanism of the EAIW. The EAIW mainly composed of porous material component, external masonry structure, and in-between air gap. Thermal insulation of the wall mainly lies in the exfiltration process within the porous material component, which can act as a heat exchanger to take advantage of the low-grade thermal energy from exhaust air for reducing the temperature difference between the inner surface of the wall and indoor air. As a result, the heat loss in winter and heat gain in summer can be significantly reduced. Previous studies indicate the exfiltration airflow within porous material can adjust the interior surface temperature of EAIW close to indoor temperature and decrease the heat gain to approximately zero despite the strong fluctuations of outdoor boundary conditions [49]. The driven force of the exfiltration airflow within porous material derives from the suction pressure of an additional mechanical fan. This multi-functional

building envelope provides an alternative solution for the in-situ utilization of the exhaust air in each conditioned room, unlike the traditional air-to-air heat exchanger that collects the exhaust air from different rooms through additional mechanical fan and air ducts.

The two-dimensional network heat transfer model proposed and validated in our previous study [37], was adopted to analyze the thermal performance and estimate the hourly cooling and heating loads of EAIW. The schematic of the two-dimensional network heat transfer model is presented in Fig. 4. The EAIW was equally segmented into several subsections in vertical direction for discretization. Each subsection consists of three components: porous material, air gap, and masonry structure. The following assumptions were used in this paper for developing the heat transfer model: (1) heat conduction between two adjacent subsections in vertical direction was neglected [50-52], (2) the possibility of condensation within the EAIW was not considered in current study, (3) long-wave radiative heat exchanger within the air gap only occurs between the two surfaces in the same subsection, (4) the porous aggregates were considered to be thermal equilibrium with the neighboring exfiltration airflow [53]. For each subsection, five governing equations for five unknown nodes temperatures can be established based on the conservation of mass and energy.

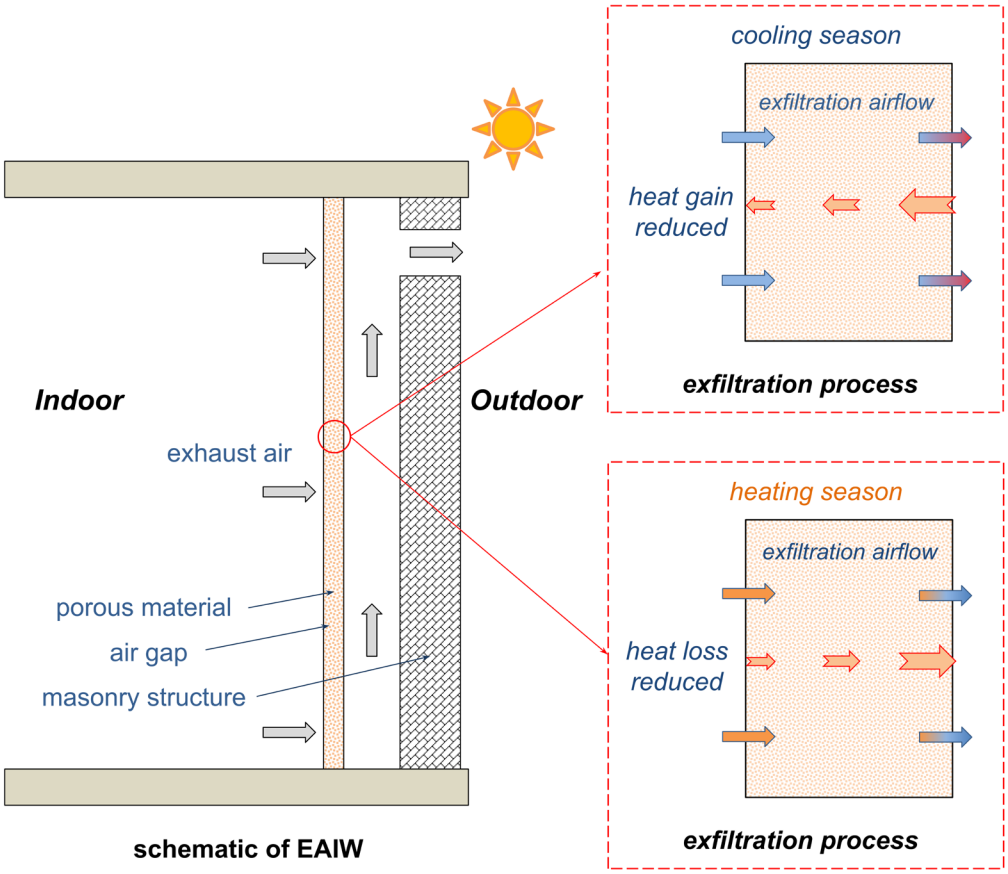

Fig. 3. Schematic and mechanism of the EAIW

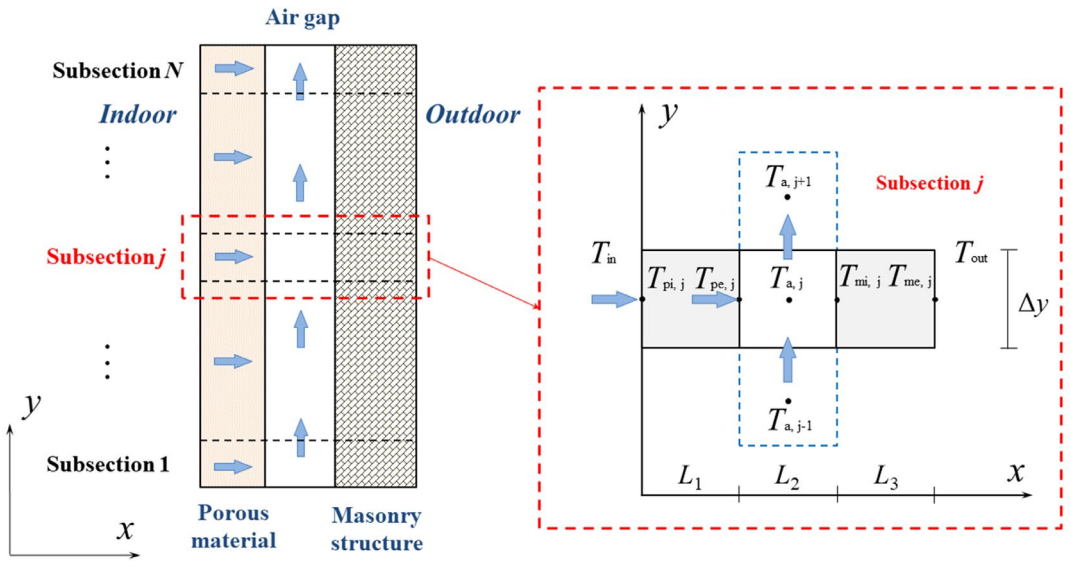

(a) Discretization in vertical direction (b) Temperature of each node in subsection j

Fig. 4. Schematic of the two-dimensional heat transfer model

For the subsection j, the one-dimensional governing equation of air-permeable porous material [53] can be expressed as Eq. (1).

$$\lambda_p \frac{\partial^2 T_{p,j}}{\partial x^2} - \rho_a c_a v \frac{\partial T_{p,j}}{\partial x} = 0 \tag{1}$$

where $T_{p,j}$ is temperature of porous material in x direction (K). The analytical expression for the temperature of porous material can be further expressed as [53]:

$$T_{p,j}(x) = \left(T_{pe,j} - T_{pi,j}\right) \cdot \frac{\exp(Ax) - 1}{\exp(AL_1) - 1} + T_{pi,j} \tag{2}$$

The conductive heat flow within porous material in x direction can be defined as Eq. (3) according to Fourier's law of heat conduction.

$$q_{c,j} = -\lambda_p \frac{\partial T_{p,j}(x)}{\partial x} \tag{3}$$

Therefore, the analytical expression for the conductive heat flow within porous material in x direction can be further expressed as follows based on the Eqs. (1) and (3).

$$q_{c,j} = -\lambda_p \frac{A\exp(Ax)}{\exp(AL_1) - 1}\left(T_{pe,j} - T_{pi,j}\right) \tag{4}$$

The governing equations for the boundary nodes of porous material can be expressed as Eqs. (5) and (6) based on the energy balance, considering the conduction within porous material, long-wave radiation, convection, and mass flow.

For the interior surface node of porous material ($x = 0$):

$$h_{ci}\left(T_{in} - T_{pi,j}\right) + \rho_a c_a v\left(T_{in} - T_{pi,j}\right) = -\lambda_p \frac{A\left(T_{pe,j} - T_{pi,j}\right)}{\exp(AL_1) - 1} \tag{5}$$

For the exterior surface node of porous material ($x = L_1$):

$$h_{ca,j}\left(T_{pe,j}-T_{a,j}\right)+h_r\left(T_{pe,j}-T_{mi,j}\right)=-\lambda_p\frac{A\exp\left(AL_1\right)}{\exp\left(AL_1\right)-1}\left(T_{pe,j}-T_{pi,j}\right) \tag{6}$$

Moreover, the governing equation for the node of air gap in subsection j can be defined as Eq. (7) considering the energy and mass balance.

$$\begin{aligned} &h_{ca,j}\left(T_{pe,j}-T_{a,j}\right)\Delta y+h_{ca,j}\left(T_{mi,j}-T_{a,j}\right)\Delta y \\ &+\rho_a c_a v T_{pe,j}\Delta y+\rho_a c_a u_{j-1}T_{a,j-1}L_2=\rho_a c_a u_j T_{a,j}L_2 \end{aligned} \tag{7}$$

The governing equations for the interior surface node ($x = L_1 + L_2$) and exterior surface node ($x = L_1 + L_2 + L_3$) of external masonry structure can be expressed as Eqs. (8) and (9) [37].

$$h_{ca,j}\left(T_{a,j}-T_{mi,j}\right)+h_r\left(T_{pe,j}-T_{mi,j}\right)+\frac{\lambda_w\left(T_{me,j}-T_{mi,j}\right)}{L_3}=0 \tag{8}$$

$$h_{ce}\left(T_{out}-T_{me,j}\right)+\frac{\lambda_m\left(T_{mi,j}-T_{me,j}\right)}{L_3}=0 \tag{9}$$

where A is model characteristic parameter and defined as: $A = (\rho_a c_a v/\lambda_p)$; c_a is the specific heat capacity of air (J/kgK); h is the heat transfer coefficient at each surface (W/m^{2}K); L_1, L_2, and L_3 are the thickness of porous material component, air gap, and masonry structure, respectively (m); T_{in} and T_{out} are the indoor temperature and outdoor solar-air temperature, respectively (K); u_{j-1} and u_j are the airflow velocities in vertical direction of air gap for the subsection j-1 and subsection j, and are expressed as: $u_{j-1}=(j-1)v\Delta y/L_2$ and $u_j=(jv\Delta y)/L_2$, respectively (m/s); v is the exfiltration velocity in horizontal direction within porous material (m/s); Δy is the height of each subsection (m); ρ_a is the air density (1.205 kg/m^3); λ_p and λ_m are the thermal conductivities of porous material and masonry structure, respectively (W/mK).

Eqs. (5) to (9) represent the governing equations of five nodes from interior surface to

exterior surface in one of the subsections. As the EAIW was segmented equally into 10 subsections for numerical simulation, therefore, 50 governing equations were established for the whole EAIW in this study. The proposed mathematical model was solved in self-developed MATLAB programs with the defined boundary conditions to obtain a converged solution. And then, the solved interior surface temperatures were used to further calculate the hourly energy demand of EAIW.

Table 1 presents the detailed information about the calculation of each heat transfer coefficient. ε_p and ε_m are the surface emissivity of porous material and masonry structure, respectively. σ represents Stefan-Boltzmann constant, and equals to 5.67×10^{-8} W/(m^{2}K^4). v_{out} is the outdoor wind speed.

Table 1 Calculation of the heat transfer coefficients

Heat transfer coefficient	Expression
At the exterior surface of EAIW [54]	$h_{\text{ce}} = 8.23 + 3.33v_{\text{out}} - 0.036v_{\text{out}}^2$
At the two surfaces of air gap [55]	$h_{\text{ca},j} = 5.62 + 3.9u_j$
At the interior surface of EAIW [56]	$h_{\text{ci}} = 8.29$
Long-wave radiation between the two surfaces within air gap	$h_r = \frac{\sigma}{\frac{1}{\varepsilon_p}+\frac{1}{\varepsilon_m}-1} \times \frac{T_{pe,j}^4 - T_{mi,j}^4}{T_{pe,j} - T_{mi,j}}$

2.2 Model validation

An experimental platform was constructed in our previous study and used to validate the above-mentioned network heat transfer model of EAIW [37]. The schematic of experiment validation is illustrated in Fig. 5 and Fig. 6. Two environment chambers were designed to

simulate the outdoor and indoor conditions. The porous material component was a 50 mm mineral wool layer. An expanded PVC panel was used as external masonry structure for simplification. Exfiltration velocity of the EAIW was controlled by a variable frequency fan. The measured exfiltration velocity and air temperatures of two chambers were the inputs of computational model. And then the measured data were compared with the corresponding simulated results. Different boundary conditions such as the variations of indoor temperature, outdoor temperature, and exfiltration velocity were considered for fully validating the computational mathematical model. The mean absolute percentage error (MAPE) and mean square error (MSE) were also used to quantitatively estimate the accuracy of computational model.

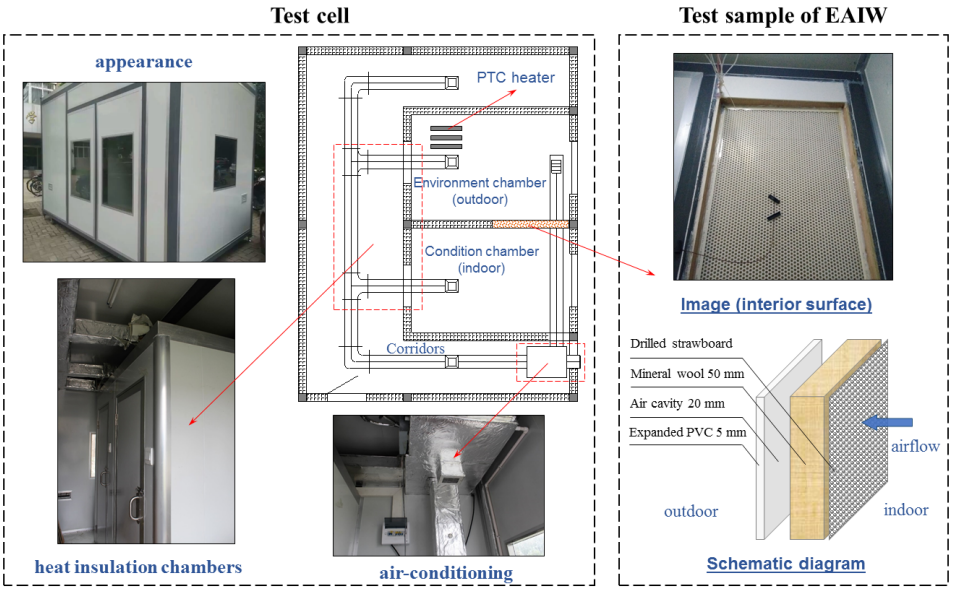

Fig. 5. Schematic of the EAIW experiment test

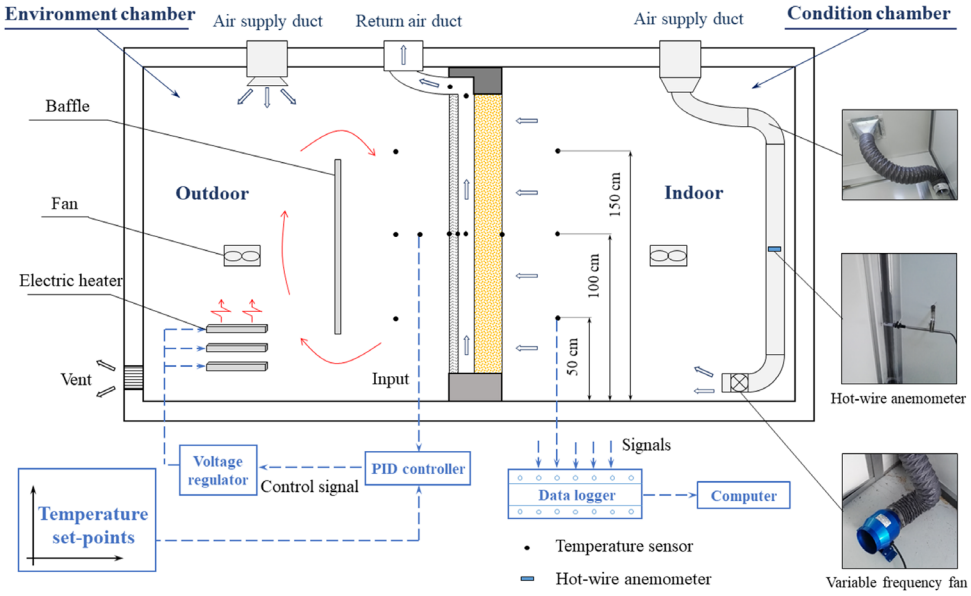

Fig. 6. Layout of the measurement instruments

The comparisons between the simulation and measurement are presented in Fig. 7. The MSE and MAPE of the simulated results are listed in Table 2. It can be found that the error in simulation outputs is quite limited. A good agreement between the measured temperatures and corresponding simulated results can be observed. As shown in the Fig. 7, the deviations of all the calculated results basically range from −0.74 ºC to 0.99 ºC. The simulated interior surface temperature of porous material shows best accuracy, and its maximum absolute deviation is only 0.38 ºC. Moreover, the MAPE for the simulated T_{pi}, T_a, T_{mi}, and T_{me} are 1.1 %, 0.9 %, 1.6 %, and 0.8 %, respectively. Therefore, it means that the developed computational model could accurately simulate and calculate the temperature of each node within EAIW. Further complete description about the experimental setup, boundary conditions, and model validation is given in Ref. [37].

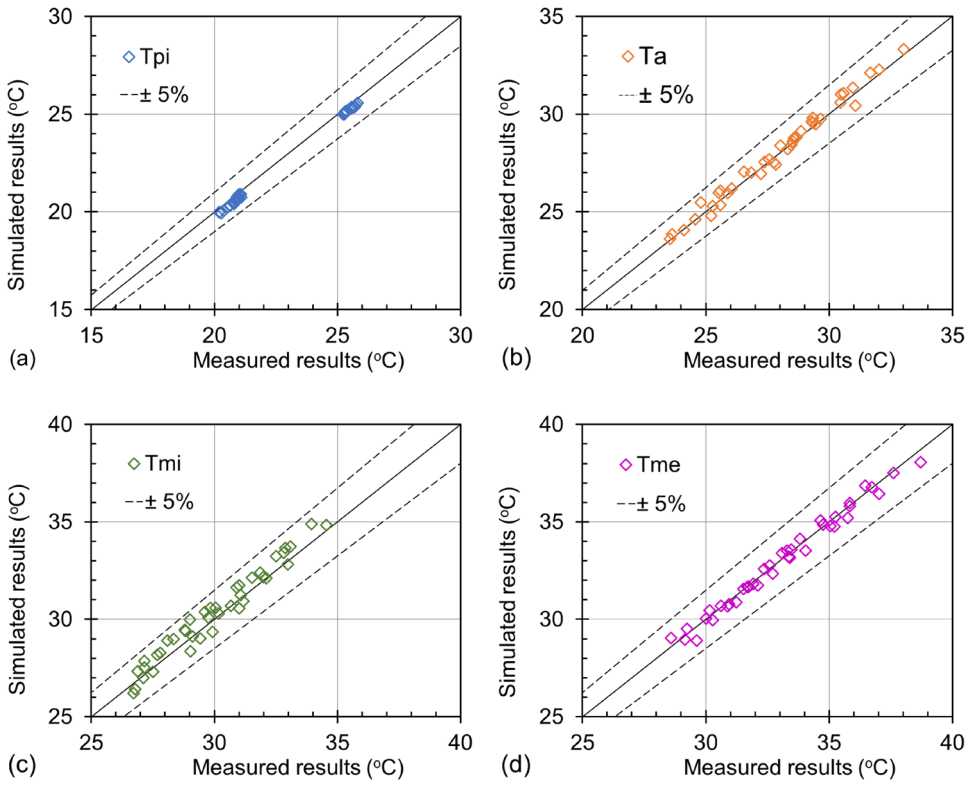

Fig. 7. Comparison of the measured data and corresponding simulated results for the: (a) interior surface of porous material; (b) ventilated air gap; (c) interior surface of external masonry structure; (d) exterior surface of external masonry structure

Table 2 Error analysis of the simulated results

Temperature	MSE	MAPE
Interior surface of porous material (T_{pi})	0.07	1.1 %
Air gap (T_a)	0.10	0.9%
Interior surface of external structure (T_{mi})	0.30	1.6 %
Exterior surface of external structure (T_{me})	0.10	0.8 %

2.3 Determining the pressure loss of exfiltration process

The driven force of exfiltration airflow is the differential pressure between indoor and outdoor. For the practical application, an additional mechanical fan is required to provide the

differential pressure and maintain a constant exfiltration airflow for EAIW. This means that the application of EAIW will lead to additional power consumption. Therefore, the pressure loss of exfiltration process and corresponding fan power consumption should be quantitatively estimated.

Darcy's law reveals the relationship between the velocity of a fluid through a permeable porous material, the permeability and thickness of porous material, the dynamic viscosity of fluid, and the pressure drop. In this study, Darcy's law was adopted to evaluate the pressure loss of exfiltration process within EAIW, as shown in Eq. (10).

$$v = \frac{k_p}{\mu}\frac{\Delta P}{L_p} \tag{10}$$

Eq. (10) can be further written as:

$$\Delta P = \frac{\mu L_p v}{k_p} \tag{11}$$

where ΔP is the pressure loss of the exfiltration airflow through the porous material (Pa); v is the exfiltration velocity (m/s); L_p is the porous material thickness (m); k_p is the permeability of porous material (m^2); μ is the dynamic viscosity of the air (Pa·s). The permeability of each porous material used in this study is derived from the Ref. [57] and presented in Table 3. The dynamic viscosity of the air is 1.81×10^{-6} Pa·s.

2.4 Evaluation index for optimal design

In this study, the annual overall energy consumption of the EAIW under different porous material thickness was calculated to identify the optimal thickness of porous material for

achieving the minimum energy consumption. The annual overall energy consumption of the EAIW is composed of the annual cooling and heating energy consumption and fan energy consumption, which can be expressed as Eq. (12).

$$E_{total} = E_c + E_h + E_{fan} \tag{12}$$

where E_{total} is the annual overall energy consumption per unit area of the EAIW (kWh/m^2); E_c and E_h are the annual electricity consumption per unit area of the EAIW for cooling and heating loads, respectively (kWh/m^2); E_{fan} is the annual electricity consumption per unit area of the EAIW for mechanical fan (kWh/m^2). Eq. (12) can further express as:

$$E_{total} = \frac{Q_c}{COP_c} + \frac{Q_h}{COP_h} + E_{fan} \tag{13}$$

where Q_c and Q_h are the cumulative cooling and heating demands of the EAIW, respectively (kWh/m^2); COP is the coefficient of performance of the air-conditioning system. An air source heat pump with assumed constant COP of 3.5 and 4.5 for space cooling and heating was selected in this study [58]. The Q_h and Q_c can be calculated by Eqs. (14) and (15), respectively.

$$Q_h = \int_{heating} h_{ci} \left(T_{in} - T_{pi} \right) d\tau \tag{14}$$

$$Q_c = \int_{\text{cooling}} h_{ci} \left(T_{pi} - T_{in} \right) d\tau \tag{15}$$

where T_{pi} is the interior surface temperature of EAIW (K); τ is the hourly time-step (h); The subscripts of heating and cooling represent the heating season and cooling season, respectively. During the year-round thermal simulation, when the interior surface temperature

of EAIW is lower than indoor temperature in cooling season or higher than indoor temperature in heating season, no cooling or heating energy was required at this time.

The annual fan power consumption per unit area of the EAIW (E_{fan}) can be expressed as Eq. (16).

$$E_{fan} = \int_{annual} \frac{G\Delta P}{1000\eta_e\eta_{fan}} d\tau \tag{16}$$

where η_e and η_{fan} are the efficiency of the electromotor and fan, and the overall efficiency of the mechanical fan ($\eta_e \times \eta_{fan}$) is assumed as 0.55 [59]; G is the volume flow rate per unit area of the EAIW (m^3/s).

3. Case study for optimal design

In this study, the EAIW was employed as the south-facing external wall of a typical office room. To identify the optimal insulation thickness of porous material, the annual overall energy consumption of EAIW under different design parameters were investigated. The typical office room was designed with a size of 6 m × 4 m × 3 m (length × width × height), and the dimension of the external wall was 4 m × 3 m (width × height). To determine its optimal value, the thickness of porous material varied from 10 mm to 200 mm with an interval of 10 mm. The results in our previous studies indicated that the external masonry structure shows limited impact on the thermal performance of the EAIW [49]. Therefore, the variation of the thickness of external masonry structure and air gap was not considered. The thickness was 20 mm for air gap and 120 mm for masonry structure, respectively. In this study, the influences of the exfiltration velocity and permeability of porous material on the optimal design and overall

annual energy performance of the EAIW were investigated quantitatively.

For the influence of permeability of porous material, two typical air-permeable porous materials (mineral wool and glass fiber) were used to quantitatively estimate the impact of porous material selection on the optimal design of the EAIW. The thermo-physical properties of the used materials are presented in Table 3.

Table 3 Thermal properties of each material [57]

Material	Thermal conductivity (W/mK)	Permeability (m^2)
Mineral wool	0.045	3.30E-10
Glass fiber	0.033	1.86E-10
Masonry structure (concrete block)	1.74	NA

The exfiltration airflow within porous material plays a significant role for preventing the unwanted conductive heat flux through EAIW. The exfiltration flow volume through EAIW was equal to the supplied fresh air volume of the conditioned office room. In this study, based on the ANSI/ASHRAE Standard 62.1-2019 [60], the ventilation fresh air rate was kept at 61.92 m^3/h for this typical office room. Moreover, the impact of the window-to-wall ratio (WWR) on the optimal design of the EAIW was also investigated. Two different WWRs of 0 % and 50 % were considered. For the situation of WWR = 0 %, the frontal area of the EAIW was 4 m × 3 m, which corresponds to a 0.00143 m/s exfiltration velocity. And the exfiltration velocity was 0.00286 m/s for the WWR = 50 %. Therefore, the exfiltration velocity of 0.00143 m/s and

0.00286 m/s was considered to identify the influence of exfiltration velocity on the optimal design of the wall.

Table 4 Detailed information of the representative cities

Climate	City	Cooling season	Heating season	Outdoor average wind speed	
				Summer	Winter
Cold zone	Beijing	Jun. 15th to Sept. 15th	Nov. 15th to Mar. 15th	2.2 m/s	2.7 m/s
HSCW zone	Wuhan	Jun. 1st to Sept. 30th	Dec. 15th to Mar. 15th	2.0 m/s	2.6 m/s
HSWW zone	Guangzhou	May 1st to Sept. 30th	Dec. 1st to Feb. 28th	1.5 m/s	2.4 m/s

The year-round thermal simulation and optimal design of the EAIW was executed in three different climate zones including HSWW zone, HSCW zone, and cold zone. In this study, three cities were selected as the representatives of three climate zones. The typical meteorological year (TMY) data of each city were obtained from weather database [61]. The cooling and heating periods of three cities have been defined by design standard of building energy efficiency [62] and are presented in Table 4. In this study, the EAIW was assumed to operate in continuous 24 hours per day throughout the whole heating and cooling seasons for simplification. The set point of indoor temperature was 25 ^{o}C in cooling season and 20 ^{o}C in heating season based on the design standard for building energy efficiency [62], respectively.

4. Results and discussion

In this study, the hourly cooling and heating load, fan power consumption as well as annual overall energy consumption of EAIW under different porous material thickness were calculated to identify the optimal value of porous material thickness, which can minimize the annual overall energy consumption of EAIW. Section 4.1 will demonstrate the existence of the optimal thickness of porous material. The influences of exfiltration velocity (0.00143 m/s and 0.00286 m/s) and porous material selection (glass fiber and mineral wool) on the optimal design will be investigated in Section 4.2 and Section 4.3, respectively. Discussion will be carried out in Section 4.4.

4.1 Determining the optimal thickness

In this subsection, the glass fiber was selected as the porous material component of the EAIW, and the WWR of 0 % was employed, corresponding to a 0.00143 m/s exfiltration velocity. The variations of the annual overall energy consumption versus thickness of porous material in different climate zones are presented in Fig. 8. The annual overall energy consumption of EAIW is composed of three components, including the energy consumption for cooling demand, heating demand, and mechanical fan.

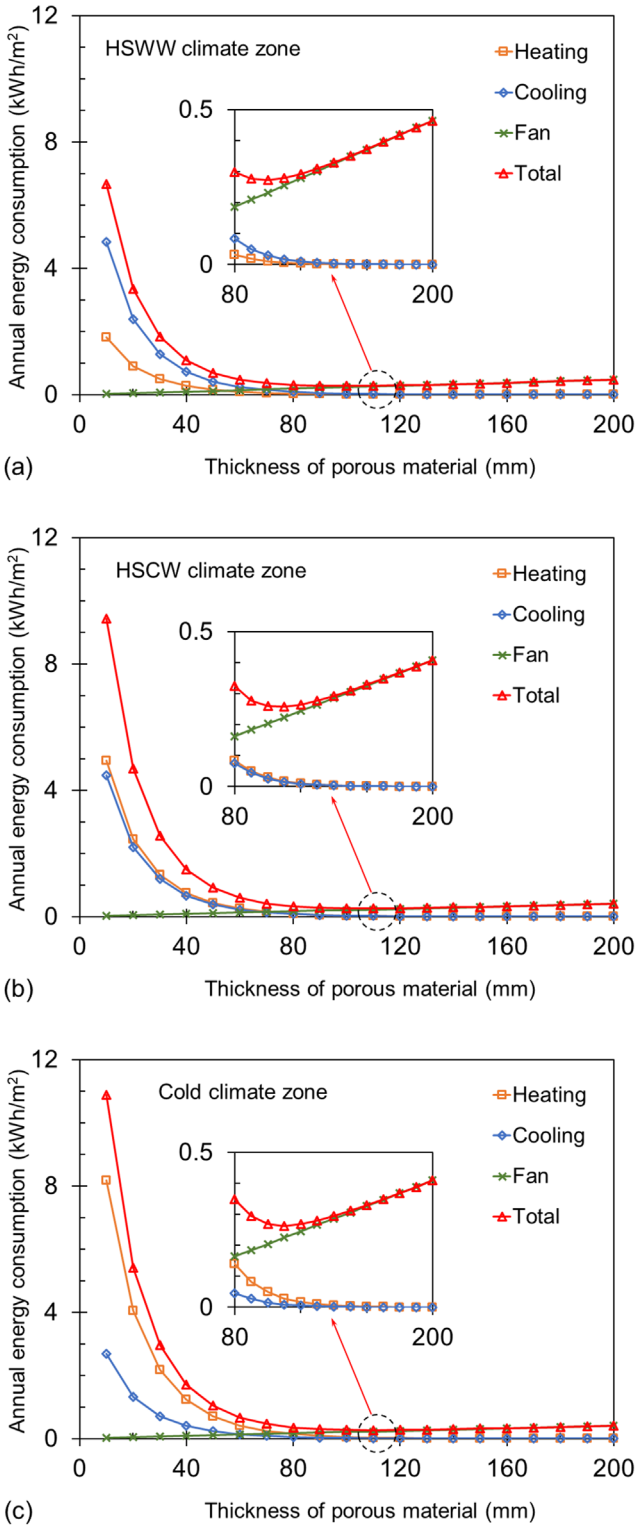

Fig. 8. Variation of annual overall energy consumption versus the thickness of porous material with a 0.00143 m/s exfiltration velocity in the climate of: (a) HSWW zone; (b) HSCW zone; (c) Cold zone

As shown in the figures, the thickness porous material shows a significant influence on

the annual cooling and heating energy consumption. The annual cooling and heating energy consumption are dramatically reduced by increasing the thickness of porous material. When the thickness of porous material varies from 10 mm to 50 mm, the annual cooling and heating energy consumption decrease from 4.83 kWh/m^2 and 1.81 kWh/m^2 to 0.42 kWh/m^2 and 0.16 kWh/m^2 for HSWW climate zone, corresponding to 91.4 % and 91.2 % reduction, respectively. Such a promising energy saving potential mainly derives from the exfiltration process of the low-grade exhaust air through the porous material component. However, the influence of porous material thickness on the cooling and heating energy consumption of EAIW is non-linear. Further increasing the thickness of porous material shows a limited reduction of annual cooling and heating energy consumption. Moreover, a linear variation of the fan energy consumption versus thickness of porous material can be observed. Such a phenomenon can be explained by Darcy' law expressed in Eq. (10). As shown in Fig. 8(a), the annual energy consumption of mechanical fan slightly increases to 0.46 kWh/m^2 when the thickness of porous material reaches to 200 mm. Similar results can also be observed in Fig. 8(b) and Fig. 8(c).

The results in Fig. 8 also reveal that there exists an optimal thickness of porous material which achieves a minimum annual total energy consumption of the EAIW. This optimal value can achieve a balance between the reduction of cooling and heating energy consumption and increase of fan energy consumption. When the thickness of porous material exceeds this optimal value, a thicker porous material component will lead to an increase of the annual total energy consumption. The optimal thickness are 100 mm, 110 mm, and 110 mm for the

HSWW, HSCW, and cold climate zones, which correspond to annual total energy consumption of 0.27 kWh/m^2, 0.26 kWh/m^2, and 0.26 kWh/m^2, respectively. Moreover, the optimal thickness for the HSWW climate zone is slightly lower than the optimal values for the HSCW and cold climate zones. This is because the cumulative cooling and heating demands of the EAIW in the HSWW climate zone is the lowest.

4.2 Influence of exfiltration velocity

In this subsection, the influence of exfiltration velocity on the optimal thickness of porous material was investigated. As the WWR varies from 0 % to 50 %, the exfiltration velocity increases from 0.00143 m/s to 0.00286 m/s. Fig. 9 presents the variations of the annual overall energy consumption versus thickness of porous material for the EAIW with a 0.00286 m/s exfiltration velocity. It can be found that compared the results in Fig. 8, the annual cooling and heating energy consumption of EAIW are significantly reduced due to the increase of exfiltration velocity. As shown in Fig. 9(a), the annual cooling and heating energy consumption are 2.72 kWh/m^2 and 1.02 kWh/m^2 for the EAIW with a porous material thickness of 10 mm. When this thickness enlarges to 50 mm, the annual cooling and heating energy consumption of EAIW decrease to approximately 0 kWh/m^2. Similar results can be obtained for other climate zones.

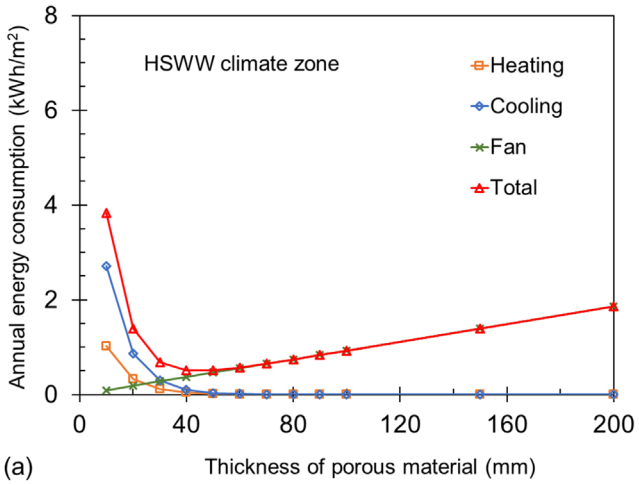

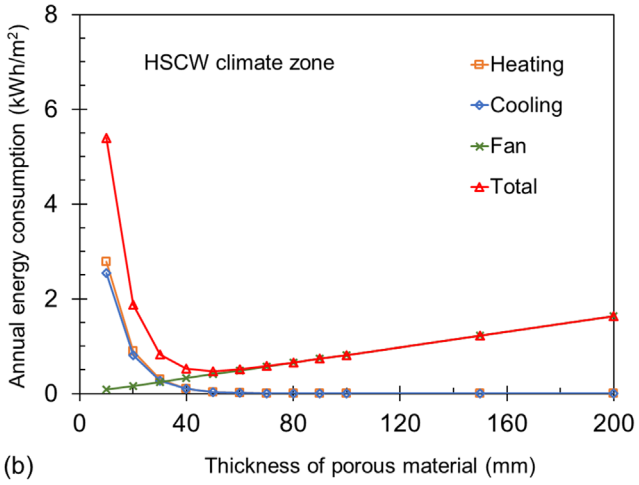

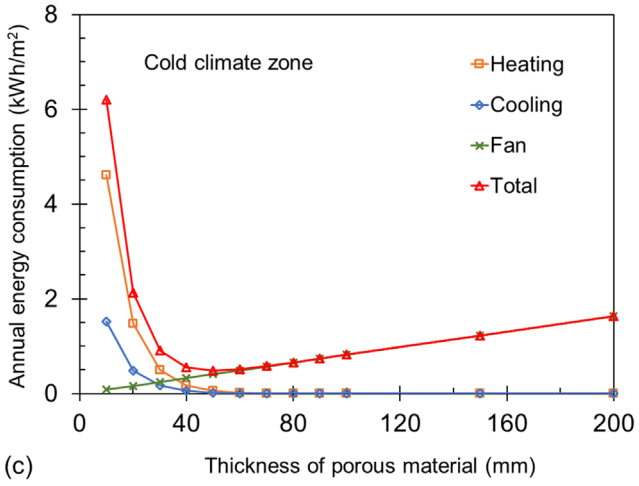

Fig. 9. Variation of annual overall energy consumption versus thickness of porous material with a 0.00286 m/s exfiltration velocity in the climate of: (a) HSWW zone; (b) HSCW zone; (c) Cold zone

However, it should be noticed that fan power consumption per unit area of EAIW exhibits a quadratic relationship with exfiltration velocity within porous material according to Eq. (16). It means that the fan energy consumption becomes a non-negligible component of the annual overall energy consumption, as the exfiltration velocity varies from 0.00143 m/s to 0.00286 m/s. The annual fan energy consumption for driving the exfiltration airflow increases to 1.86 kWh/m^2 for the EAIW with 200 mm porous material, as shown in Fig. 9(a). To achieve a compromise between the cooling, heating and fan energy consumption, the optimal thickness of porous material are 40 mm, 50 mm, and 50 mm for the EAIW, which can minimize the annual overall energy consumption to 0.51 kWh/m^2, 0.48 kWh/m^2, and 0.49 kWh/m^2 in the HSWW, HSCW, and cold climate zones, respectively.

This can be concluded that for the EAIW with a higher exfiltration velocity, the minimum value of annual overall energy consumption may slightly increase due to the influence of additional fan energy consumption. Moreover, a lower optimal value can be observed for the porous material thickness.

4.3 Influence of porous material selection

In this subsection, the influence of porous material selection on the optimal thickness of porous material was quantitatively evaluated. Based on the previous studies on air-permeable building envelope, two commonly used porous materials (glass fiber and mineral wool) were selected and compared. Compared to mineral wool, glass fiber has a lower thermal conductivity and permeability (as shown in Table 3).

Fig. 10 and Fig. 11 illustrate the annual overall energy consumption of EAIW with different porous materials. The results show significant difference between the annual overall energy consumption of EAIW with different porous materials. For the EAIW with a 0.00286 m/s exfiltration velocity, the optimal thickness of mineral wool are 60 mm, 70 mm, and 70 mm in the HSWW, HSCW, and cold climate zones. Owing to the lower permeability of glass fiber, the application of glass fiber will decrease the optimal thickness to 40 mm, 50 mm, and 50 mm, respectively. This is because that a lower permeability leads to a higher pressure loss as well as additional fan power consumption, which will increase the influence of fan energy consumption on the overall energy consumption and then result in a downward trend of the optimal thickness.

For a 0.00286 m/s exfiltration velocity, moreover, the minimum annual overall energy consumption of EAIW with mineral wool are 0.41 kWh/m^2, 0.38 kWh/m^2, and 0.39 kWh/m^2 in the HSWW, HSCW, and cold climate zones, respectively. Despite glass fiber has a lower thermal conductivity, using glass fiber as air-permeable component will increase these minimum values to 0.51 kWh/m^2, 0.48 kWh/m^2, and 0.49 kWh/m^2, respectively. It can be concluded that permeability of porous material component shows a significant influence on the overall energy performance of EAIW. A porous material with too low permeability is detrimental to minimize the annual overall energy consumption of EAIW. Therefore, a porous material with low thermal conductivity and high permeability is highly recommended as the air-permeable component of the EAIW.

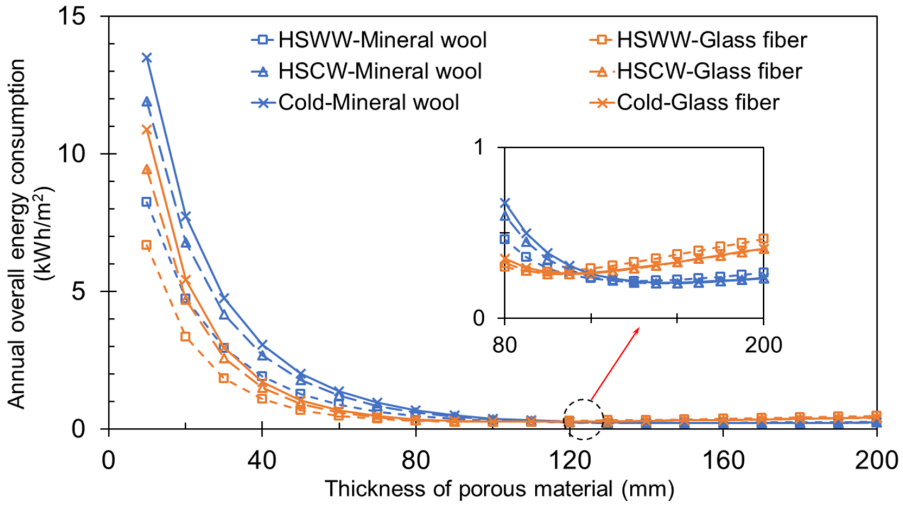

Fig. 10. Annual overall energy consumption of EAIW with two different porous materials for a 0.00143 m/s exfiltration velocity (WWR of 0 %)

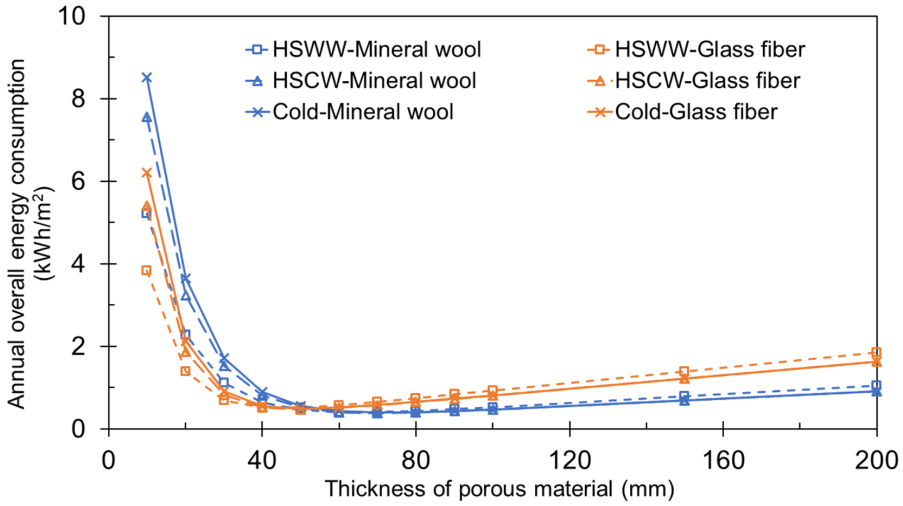

Fig. 11. Annual overall energy consumption of EAIW with two different porous materials for a 0.00286 m/s exfiltration velocity

4.4 Discussion

The above results indicate that the exfiltration process of the EAIW will lead to pressure loss as well as additional fan power consumption to a certain degree. More importantly, this study demonstrates the existence of the optimal thickness of porous material component, which can achieve a minimum annual total energy consumption of the EAIW. However,

previous studies about EAIW have not considered the pressure loss of exfiltration process and its impact on the overall energy performance of EAIW. This means that previous studies may overestimate the energy saving potential of the wall. As shown in Fig. 9(a), the annual energy consumption of cooling and heating demand is 0.14 kWh/m^2 for the EAIW with 40 mm porous material. This annual energy consumption will increase to 0.51 kWh/m^2 when the cooling, heating, and additional fan energy consumption are simultaneously considered. In this case, the energy consumption of additional fan is even higher than that for cooling and heating.

Moreover, increasing the thickness of porous material has been proven to be one of the major approaches to reduce the U-value and eliminate the heat loss or heat gain of air-permeable building envelope. A thicker porous material component indeed can significantly reduce the cooling and heating energy consumption of air-permeable building envelope. The above studies demonstrate the existence of the optimal thickness of porous material when considering the impact of pressure loss. This means that as the thickness of porous material exceeds this optimal value, it will result in a higher overall energy consumption. As shown in Fig. 9(a), when the porous material thickness varies from the optimal value (40 mm) to 100 mm, the annual overall energy consumption of EAIW increases from 0.51 kWh/m^2 to 0.93 kWh/m^2. For the design and performance evaluation of EAIW, therefore, the influence of pressure loss of exfiltration or infiltration process can not be neglected.

Previous studies mainly concern the thermal conductivity of porous material and its

impact on the thermal performance of EAIW, and neglect the influence of permeability of porous material. The above-mentioned results indicate that permeability of porous material shows a significant impact on the energy performance and design of EAIW. Despite only considering two kinds of porous materials, it can be deduced that the materials with high permeability and thermal resistance are recommended for the air-permeable component of EAIW.

Furthermore, it should be noticed that the main purpose of this study is to propose a methodology to identify the optimal thickness of porous material for minimizing the overall energy consumption of EAIW. This study only quantitatively investigates the influence of exfiltration velocity and porous material selection on the optimal design of EAIW for illustrating how key parameters impact the optimal design. But, there exist some other factors that would potentially impact this optimal design to a certain degree. For instance, the set point of air temperature in cooling and heating season may affect the optimal thickness of porous material. In this study, these set points for numerical simulation are adopted based on design standard for building energy efficiency. When the set point of air temperature increases in cooling season or decreases in heating season, predictably, it would result in a downward trend for the optimal thickness of EAIW. This is mainly because such a variation of set point would reduce the cooling and heating loads of the EAIW, which may increase the proportion of fan energy consumption in overall energy consumption of EAIW. Meanwhile, the exfiltration flow volume through the EAIW is equal to the supplied fresh air volume, which varies depending on the building category and occupant number. This means that the

optimal design of EAIW would also be influenced by building category.

5. Conclusions and outlook

The EAIW is a kind of multi-functional air-permeable building envelope, which can provide an alternative solution for in-situ utilization of the exhaust air in each conditioned room to improve the thermal insulation of building envelope. In this study, a methodology for optimizing the design parameter of porous material component was proposed for maximizing the energy saving potential of EAIW. A network heat transfer model was developed and validated for analyzing the hourly thermal performance of EAIW. A Darcy's law-based pressure loss model was proposed to evaluate the pressure loss of the exfiltration process within EAIW, and to further estimate the additional fan power consumption for providing a stable exfiltration airflow. A sensitive analysis was conducted to investigate the influence of porous material thickness on the overall energy consumption of EAIW, and then the optimal thickness of porous material component was identified to achieve the minimum overall energy consumption. Different scenarios were also considered. The main conclusions can be summarized as follows.

(1) The optimal thickness of porous material component has been identified for EAIW. This optimal value achieves a trade-off between the cooling/heating energy consumption and additional fan power consumption, which can minimize the annual overall energy consumption of EAIW.

(2) The exfiltration velocity shows a significant influence on the additional fan power

consumption and optimal thickness of porous material component. When the velocity varies from 0.00143 m/s to 0.00286 m/s, the optimal thickness will decrease from 100 mm, 110 mm, and 110 mm to 40 mm, 50 mm, and 50 mm in the HSWW, HSCW, and cold climate zones, respectively. However, the minimum annual overall energy consumption of EAIW may slightly increase due to the influence of additional fan energy consumption.

(3) For the air-permeable building envelope, the influence of permeability of porous material component cannot be neglected. The results show that a lower permeability of porous material leads to a higher pressure loss, which is detrimental to minimize the overall energy consumption of EAIW. For the purpose of energy saving, the porous material with high permeability and low thermal conductivity is strongly recommended for the EAIW.

(4) The pressure loss of exfiltration process should be considered when estimating the energy saving potential of EAIW. Otherwise, the cooling and heating loads of the EAIW will be underestimated.

The EAIW provides an alternative solution for in-situ utilizing and recovering the low-grade exhaust air. However, it should be noticed that such a kind of building envelope only utilizes the sensible heat of exhaust air. In future work, utilization of the latent heat of exhaust air will be further explored for the EAIW. The energy, economy, environmental performance of the EAIW and conventional mechanical ventilation heat recovery system should be compared under different scenarios to clarify whether or not the use of EAIW is

better than conventional exhaust air heat recovery system from multi-perspective. Moreover, the possibility of condensation in winter and its corresponding prevention measure should be investigated to explore the technical feasibility and design guideline of EAIW in severe cold climate.

The EAIW is originally proposed for utilizing the indoor exhaust air to prevent the heat gain or loss through the wall. This means that this wall currently only applies to the buildings installed with fresh air ventilation system. The previous studies indicate the outstanding thermal performance of EAIW mainly derives from the exfiltration process of low-grade exhaust air through the porous layer. Such an exfiltration insulation mechanism can be further integrated with passive natural ventilation driven by stack effect in hot-dry climate or other low-grade energy sources such as earth-to-air heat exchanger. Further exploration of integrating the exfiltration insulation with other energy-efficient technologies is deserved.

Acknowledgement

This research has received the support from the grants of the National Natural Science Foundation of China (Grant Nos. 51808239 and 51378231) and Hong Kong Scholars Program (grant number XJ2019044).

CRediT author statement

Chong Zhang: Methodology, Investigation, Formal analysis, Data curation, Visualization, Writing-original draft preparation, Writing-review and editing. **Jinbo Wang**: Conceptualization, Supervision, Funding acquisition, Writing-review and editing. **Fu Xiao**: Supervision, Writing-review and editing.

Declaration of competing interest

The authors declare that they have no known competing financial interests or personal relationships that could have appeared to influence the work reported in this paper.

References

[1] IEA, World Energy Statistics and Balances 2018, OECD/IEA, Paris, 2018.

[2] Zhang C, Cui C, Zhang Y, Yuan J, Luo Y, Gang W. A review of renewable energy assessment methods in green building and green neighborhood rating systems. Energy Build 2019, 195: 68-81.

[3] Ran S, Lyu W, Li X, Xu W, Wang B. A solar-air source heat pump with thermosiphon to efficiently utilize solar energy. J Build Eng 2020, 31: 101330.

[4] Nik-Bakht M, Panizza RO, Hudon P, Chassain PY, Bashari M. Economy-energy trade off automation–A decision support system for building design development. J Build Eng 2020, 30: 101222.

[5] Li A, Xiao F, Zhang C, Fan C. Attention-based interpretable neural network for building cooling load prediction. Appl Energy 2021, 299: 117238.

[6] Haddad S, Synnefa A, Marcos MÁP, Paolini R, Delrue S, Prasad D, Santamouris M. On the potential of demand-controlled ventilation system to enhance indoor air quality and thermal condition in Australian school classrooms. Energy Build 2021, 238, 110838.

[7] Zhang C, Gang W, Wang J, Xu X, Du Q. Numerical and experimental study on the thermal performance improvement of a triple glazed window by utilizing low-grade exhaust air. Energy 2019, 167: 1132-1143.

[8] Sadineni SB, Madala S, Boehm RF. Passive building energy savings: A review of building envelope components. Renew Sust Energ Rev 2011, 15: 3617-3631.

[9] Khoukhi M, Abdelbaqi S, Hassan A. Transient temperature change within a wall embedded insulation with variable thermal conductivity. Case Stud Therm Eng 2020, 20: 100645.

[10] Liu Y, Wu H, Zhang Y, Yang J, He F. Structure characteristics and hygrothermal performance of silica aerogel composites for building thermal insulation in humid areas. Energy Build 2020, 228: 110452.

[11] Hung Anh LD, Pásztory Z. An overview of factors influencing thermal conductivity of building insulation materials. J Build Eng 2021, 44: 102604.

[12] Pirasaci T. Investigation of phase state and heat storage form of the phase change material (PCM) layer integrated into the exterior walls of the residential-apartment during heating season. Energy 2020, 207: 118176.

[13] Ramakrishnan S, Pasupathy K, Sanjayan J. Synthesis and properties of thermally enhanced aerated geopolymer concrete using form-stable phase change composite. J Build Eng 2021, 44: 102756.

[14] Zhang S, Hu W, Li D, Zhang C, Arıcı M, Yıldız, Ç, et al. Energy efficiency optimization of PCM and aerogel-filled multiple glazing windows. Energy 2021, 222: 119916.

[15] Lee LSH, Jim CY. Energy benefits of green-wall shading based on novel-accurate apportionment of short-wave radiation components. Appl Energy 2019, 238: 1506-1518.

[16] La Roche P, Yeom DJ, Ponce A. Passive cooling with a hybrid green roof for extreme climates. Energy Build 2020, 224: 110243.

[17] Arıcı M, Tükel M, Yıldız Ç, Li D, Karabay H. Is the thermal transmittance of air-filled inclined multi-glazing windows similar to that of vertical ones?. Energy Build 2020, 229: 110515.

[18] Arıcı M, Karabay H, Kan M. Flow and heat transfer in double, triple and quadruple pane windows. Energy Build 2015, 86: 394-402.

[19] Tükel M, Mumcuoğlu K, Arıcı M, Karabay H. Analysis of fluid flow and heat transfer characteristics in multiple glazing roofs with a special emphasis on the thermal performance. Appl Therm Eng 2019, 148: 694-703.

[20] Li A, Xu X, Sun Y. A study on pipe-embedded wall integrated with ground source-coupled heat exchanger for enhanced building energy efficiency in diverse climate regions. Energy Build 2016, 121: 139-151.

[21] Yan T, Li J, Gao J, Xu X, Yu J. Model validation and application of the coupled system of pipe-encapsulated PCM wall and nocturnal sky radiator. Appl Therm Eng 2021, 194: 117057.

[22] Shen C, Li X. Dynamic thermal performance of pipe-embedded building envelope utilizing evaporative cooling water in the cooling season. Appl Therm Eng 2016, 106: 1103-1113.

[23] Shen C, Li X. Energy saving potential of pipe-embedded building envelope utilizing low-temperature hot water in the heating season. Energy Build 2017, 138: 318-331.

[24] Lyu W, Li X, Yan S, Jiang S. Utilizing shallow geothermal energy to develop an energy efficient HVAC system. Renew Energy 2020, 147: 672-682.

[25] Zhao D, Aili A, Zhai Y, Xu S, Tan G, Yin X, et al. Radiative sky cooling: Fundamental principles, materials, and applications. Appl Phys Rev 2019, 6: 021306.

[26] Chen J, Lu L. Comprehensive evaluation of thermal and energy performance of radiative roof cooling in buildings. J Build Eng 2021, 33: 101631.

[27] Zhai Y, Ma Y, David SN, Zhao D, Luo R, Tan G, et al. Scalable-manufactured randomized glass-polymer hybrid metamaterial for daytime radiative cooling. Science 2017, 355: 1062-1066.

[28] Zhao DL, Aili A, Yin, X, Tan G, Yang R. Roof-integrated radiative air-cooling system to achieve cooler attic for building energy saving. Energy Build 2019, 203: 109453.

[29] Gholami H, Røstvik HN. Economic analysis of BIPV systems as a building envelope material for building skins in Europe. Energy 2020, 204: 117931.

[30] Buratti C, Palladino D, Moretti E, Palma RD. Development and optimization of a new ventilated brick wall: CFD analysis and experimental validation. Energy Build 2018, 168: 284-297.

[31] Zhang C, Wang J, Li L, Wang F, Gang, W. Utilization of earth-to-air heat exchanger to pre-cool/heat ventilation air and its annual energy performance evaluation: A case study. Sustainability 2020, 12: 8330.

[32] Huang J, Yu J, Yang H. Effects of key factors on the heat insulation performance of a hollow block ventilated wall. Appl Energy 2018, 232: 409-423.

[33] Wang J, Du Q, Zhang C, Xu X, Gang W. Mechanism and preliminary performance analysis of exhaust air insulation for building envelope wall. Energy Build 2018, 173: 516-529.

[34] Alongi A, Angelotti A, Mazzarella L. A numerical model to simulate the dynamic performance of Breathing Walls. J Build Perform Simu 2021, 14(2): 155-180.

[35] Dalehaug A. Development and survey of a wall construction using dynamic insulation. Building Physics93 3rd Nordic Symposium, Lyngby, Denmark, 1993, 1: 219-226.

[36] Taylor BJ, Imbabi MS, The application of dynamic insulation in buildings. Renew Energy 1998, 15: 377–382.

[37] Zhang C, Gang W, Xu X, Li L, Wang J. Modelling, experimental test, and design of an active air permeable wall by utilizing the low-grade exhaust air. Appl Energy 2019, 240: 730-743.

[38] Dimoudi A, Androutsopoulos A, Lykoudis S. Experimental work on a linked, dynamic and ventilated, wall component. Energy Build 2004, 36: 443-453.

[39] Gan G. Numerical evaluation of thermal comfort in rooms with dynamic insulation. Build Environ 2000, 35: 445-453.

[40] Wong JM, Glasser FP, Imbabi MS. Evaluation of thermal conductivity in air permeable concrete for dynamic breathing wall construction. Cem Concr Compos 2007, 29: 647-655.

[41] Di Giuseppe E, D'Orazio M, Di Perna C. Thermal and filtration performance assessment of a dynamic insulation system. Energy Proc 2015, 78: 513-518.

[42] Taylor BJ, Webster R, Imbabi MS, The building envelope as an air fiter. Build Environ 1999, 34: 353–361.

[43] Ascione F, Bianco N, Stasio CD, Mauro GM, Vanoli GP. Dynamic insulation of the building envelope: numerical modeling under transient conditions and coupling with nocturnal free cooling. Appl Therm Eng 2015, 84: 1–14.

[44] Alongi A, Angelotti A, Mazzarella. Experimental investigation of the steady state behaviour of Breathing Walls by means of a novel laboratory apparatus. Build Environ 2017, 123: 415-426.

[45] Alongi A, Angelotti A, Mazzarella L. Measuring a Breathing Wall's effectiveness and dynamic behaviour. Indoor Built Environ 2020, 29: 783-792.

[46] Alongi A, Angelotti A, Mazzarella L. Experimental validation of a steady periodic analytical model for Breathing Walls. Build Environ 2020, 168: 106509.

[47] Craig S, Grinham J. Breathing walls: The design of porous materials for heat exchange and decentralized ventilation. Energy Build 2017, 149: 246-259.

[48] Craig S, Halepaska A, Ferguson K, Rains P, Elbrecht J, Freear A, et al. The design of mass timber panels as heat-exchangers (dynamic insulation). Front Built Environ 2021, 6: 606258.

[49] Zhang C, Wang J, Li L, Gang W. Dynamic thermal performance and parametric analysis of a heat recovery building envelope based on air-permeable porous materials. Energy 2019, 189: 116361.

[50] Zanghirella F, Perino M, Serra V. A numerical model to evaluate the thermal behaviour of active transparent facades. Energy Build 2011, 43: 1123–1138.

[51] Zhang C, Wang J, Li L, Gang W. Condensation risk of exhaust air heat recovery window system: Assessment, key parameters, and prevention measure. Case Stud Therm Eng 2021, 24: 100830.

[52] Wang Y, Chen Y, Li C. Airflow modeling based on zonal method for natural ventilated double skin façade with Venetian blinds. Energy Build 2019, 191: 211-223.

[53] Taylor BJ, Cawthorne DA, Imbabi MS. Analytical investigation of the steady-state behaviour of dynamic and diffusive building envelopes. Build Environ 1996, 31: 519-525.

[54] Mirsadeghi M, Costola D, Blocken B, Hensen JLM. Review of external convective heat transfer coefficient models in building energy simulation programs: Implementation and uncertainty. Appl Therm Eng 2013, 56: 134-151.

[55] McAdams WH. Heat transmission. 3rd ed. New York: McGraw-Hill; 1954.

[56] ASHRAE. ANSI/ASHRAE Standard 140-2017, Standard method of test for the evaluation of building energy analysis computer programs. Atlanta, GA: American Society of Heating, Refrigerating and Air-Conditioning Engineers, Inc, 2017.

[57] Kumaran MK. IEA-Annex 24 on Heat, air and moisture transfer in insulated envelope parts: task 3 material properties, final report, Leuven, 1996.

[58] Chow TT, Liu W. Warm climate performance of water-filled double-glazing with submerged heat exchanger. Sustain Cities Soc 2020, 58: 102135.

[59] El Fouih Y, Stabat P, Rivière P, Hoang P, Archambault V. Adequacy of air-to-air heat recovery ventilation system applied in low energy buildings. Energy Build 2012, 54: 29-39.

[60] ASHRAE. ANSI/ASHRAE Standard 62.1-2019, Ventilation for acceptable indoor air quality. Atlanta, GA: American Society of Heating, Refrigerating and Air-Conditioning Engineers, Inc, 2019.

[61] China Meteorological Bureau, Climate Information Center, Climate Data Office and Tsinghua University, Department of Building Science and Technology. China standard weather data for analyzing building thermal conditions. China Architecture and Building Press, Beijing, 2005.

[62] Ministry Housing and Urban-Rural Development of People's Republic of China. Design standard for energy efficiency of public buildings (GB50189-2015). Beijing, China: Architecture & Building Press; 2015.